Enhanced photon utilization in single cavity mode air-bridge

thermophotovoltaic cells

Jihun Lim<sup>a</sup>, Bosun Roy-Layinde<sup>b</sup>, Bin Liu<sup>a</sup>, Andrej Lenert <sup>b</sup>, and Stephen R. Forrest<sup>a,c,1</sup>

<sup>a</sup>Department of Electrical Engineering and Computer Science, University of Michigan, Ann

Arbor, MI 48109

<sup>b</sup>Department of Chemical Engineering, University of Michigan, Ann Arbor, MI 48109

<sup>c</sup>Department of Physics and Materials Science and Engineering, University of Michigan, Ann

Arbor, MI 48109

<sup>1</sup>Corresponding author email: stevefor@umich.edu

**Keywords** 

thermophotovoltaics, thin-film membrane, photon recycling, renewable energy, III-V

compounds

**Abstract** 

An air-bridge thermophotovoltaic (TPV) cell can enable nearly complete utilization of out-of-

band (OOB) photons. However, the air-bridge consists of a micron-thick free-standing

semiconductor membrane that can buckle during fabrication. Such a buckled membrane

supports multiple optical cavity modes in the air gap between the semiconductor and the

bottom, metal back surface reflector, causing up to 10% loss in OOB reflectance ( $R_{OOB}$ ). Here

we demonstrate a single cavity mode with an extremely flat In<sub>0.53</sub>Ga<sub>0.47</sub>As TPV membrane that

exhibits  $R_{OOB} = 98.9 \pm 0.1\%$  under 1352 K blackbody illumination. The remaining 1.1%

reflectance loss is attributed to free carrier absorption and cavity oscillations. The flat TPV cell

exhibits a spectral efficiency ranging from 68.6 % to 76.5 % for emitter temperatures between

900–1500 K, which exceeds that of previous reflective TPV cells, and represents a 20-30%

1

improvement compared to the buckled cell, leading to a power conversion efficiency of 31.7  $\pm$  0.1 % at 1352 K.

#### Introduction

According to recent reports, the share of fossil fuels in global energy consumption is greater than  $80\%^{-1}$ . Renewable energy sources are critical to reducing this share, thereby decreasing greenhouse gas emissions and reducing the impact on climate change  $^{2-5}$ . Among different renewable sources, solar energy harvesting has gained an increasing share of commercial electricity production capacity, although it remains limited to  $< 10\%^{-4, 6, 7}$ . In this context, the integration of thermophotovoltaic (TPV) devices into power grids can harvest electrical power from both waste and stored (e.g., thermal battery) heat sources  $^{8-11}$ .

The coupling of a reflector to a TPV cell facilitates effective recycling of unabsorbed below-bandgap, or out-of-band (OOB) photons thereby maximizing the TPV power conversion efficiency (PCE)  $^{12\text{-}16}$ . Recently, we have shown that nearly lossless Fresnel reflection can be achieved by introducing an air gap whose thickness is on the order of a wavelength, between the Au back surface reflector (BSR) and the cell active layer  $^{16$ ,  $^{17}$ . However, such thin-film membranes are vulnerable to strain, resulting in mechanical distortion and structural failures such as cracks  $^{18}$ . In this work, we analyze the multiple optical modes supported by a buckled,  $In_{0.53}Ga_{0.47}As$  thin-film air-bridge membrane, reducing  $R_{OOB}$  by as over 10%. To mitigate this loss, we demonstrate flat cavities that support only a single mode by stiffening the membrane using a conductive, transparent epitaxial layer. We use Fourier-transform infrared (FTIR) spectroscopy to measure the optical performance of the cells, and we quantify the electrical characteristics when illuminated by a SiC heat source. The flat cell demonstrates a spectral efficiency (SE) of 74.1 % for a 1352 K emitter temperature, with an open-circuit voltage ( $V_{oc}$ ),

fill-factor (FF), and PCE of  $445.4 \pm 0.2$  mV,  $72.4 \pm 0.1$  %, and  $31.7 \pm 0.1$  %, respectively. By assuming a modestly improved diode performance that minimizes nonradiative recombination, we estimate that the single mode air-bridge TPV (ABTPV) structure can reach an efficiency of 40.2% under a 1523 K blackbody spectrum.

### **Results and Discussion**

Figure 1(a) illustrates the schematic of a buckled In<sub>0.53</sub>Ga<sub>0.47</sub>As ABTPV cell <sup>16</sup>. The TPV membrane thickness is 1.4 $\mu$ m, and the air-bridge spacing width ( $W_{air}$ ) is 80 $\mu$ m. The buckled morphology results from Au-Au thermocompression bonding of the epilayer to a host substrate <sup>18</sup>. The membrane forms an optical cavity with the bottom Au mirror, resulting in cavity modes apparent in its reflection spectrum, and parasitic reflection losses at the OOB wavelengths. Figure 1(b) shows confocal laser microscope images of the downward buckled  $In_{0.53}Ga_{0.47}As$  TPV cell (see Methods) with a nominal buckling height of  $t_{buck} = 450$  nm. The buckled membrane causes the variation of the air-bridge thickness from  $t_{air,max} = 500$  nm at the edge, to  $t_{air,min}$  = 50 nm at the center. The existence of multiple optical modes in the deformed cavity broadens the transmission peaks compared to a single cavity mode supported by an uniform air-bridge thickness of  $t_{air} = 500$  nm. The top and middle panels in Fig. 1(c) show the measured and simulated spectrum for the buckled sample, while the bottom panel shows the simulation for a flat structure. In the calculations, the imaginary refractive index (k) includes free carrier absorption (FCA) based on Drude theory (see Methods and Supplementary Information). Note that the simulation for the buckled structure, which is the sum over all cavity modes with thicknesses from  $t_{air} = 50$  to 500 nm, agrees with the experimental data. This reveals that the reflectance is decreased in the buckled membrane compared with a flat membrane (bottom panel in Fig. 1(c), resulting in a concomitant loss in  $R_{OOB}$ .

The effect of buckling can be suppressed by increasing the thickness, and hence the stiffness of the TPV membrane ( $t_{TPV}$ ), which is a function of the slenderness ratio,  $W_{air}/t_{TPV}$ . <sup>18</sup> To reduce buckling, the membrane thickness is increased from 1.4 $\mu$ m to 3.4 $\mu$ m by including a 2- $\mu$ m-thick, n-type InP buffer layer during growth, as depicted in Fig. 2(a). The electron mobility in InP is 3000 <  $\mu_e$  < 5500 cm<sup>2</sup>/Vs depending on the doping concentration. With its relatively high mobility and a carrier concentration >  $10^{16}$ /cm<sup>3</sup>, the addition of the buffer layer has no significant effect on the diode series resistance of  $R_s = 7 - 26$  m $\Omega \cdot$  cm<sup>2</sup> <sup>16, 19</sup> (see the Supporting Information). In our case, the molecular beam epitaxially (MBE)-grown buffer layer has a relatively low carrier concentration of  $3 \times 10^{16}$ /cm<sup>3</sup>, <sup>20, 21</sup> which also results in a low FCA.

Figure 2(b) is a micrograph of an In<sub>0.53</sub>Ga<sub>0.47</sub>As ABTPV cell that includes the thick InP buffer layer. The dashed line indicates the area of the membrane forming the air bridge. Figure 2(c) is the surface profilometry measurement through the membrane, indicated by the dashed line in the inset. The profile shows the relative flatness of the TPV compared to the buckled membrane in Fig. 1(b). In the Supporting Information, we characterize In<sub>0.53</sub>Ga<sub>0.47</sub>As ABTPV cells with several different diameters, where the suppression of the buckled morphology is enabled regardless of membrane size for a fixed air-bridge spacing.

To quantify the improvement in optical performance of the flat membrane structure, we compare its simulated and measured reflectance to that of a buckled membrane in Fig. 3(a). The shaded background and the solid red line represent the simulated reflectances of the flat membrane with  $t_{air} = 600$  nm without or with FCA, respectively. The dashed line (black) is the measured reflectance for the buckled membrane shown in Fig. 1. The experimental results for the flat membrane (blue circles) are close to simulations, implying that the flat TPV cell supports only a single cavity mode. At wavelengths > 5  $\mu$ m (< 0.25 eV), FCA significantly

reduces the reflectance. However, the  $R_{OOB}$  loss by FCA is negligible when the reflectance is weighted by the > 1000 K blackbody spectrum. The measured  $R_{OOB} = 97.4 \pm 0.1$  % at wavelengths of  $1.72 - 15.4 \mu m$ . When weighted to a 1352 K blackbody spectrum,  $R_{OOB}$ increases to  $98.9 \pm 0.1\%$ . The improvement in  $R_{OOB}$  by the flat membrane can be directly translated to an increased SE, as shown in Fig. 3(b). The dashed lines are the simulations, where the blue shaded region shows losses due to FCA, which become significant at a relatively low emitter temperature. The red solid lines are the measured minimum to maximum values of SE arising from uncertainties in the FTIR measurements over the range of 1 - 15.4 µm. The omission of energies > 1.24 eV can result in inaccuracies at temperatures higher than those shown. Using simulations in Fig. 3(a), we calculate the FTIR spectrum from  $0.4 - 20 \mu m$ , which is plotted in the blue shaded region in Fig. 3(b). Compared to the flat TPV cell, the buckled cell in Fig. 1(d) shows a relative decrease in SE of  $\geq$  20 – 30% at  $T_h \leq$  1400K due to the presence of multiple cavity modes (dash-dotted line). The data points are previously reported spectral efficiencies for In<sub>0.53</sub>Ga<sub>0.47</sub>AsTPV cells<sup>12, 16</sup>, which exhibit a significantly lower SE compared to the flat, single-cavity mode In<sub>0.53</sub>Ga<sub>0.47</sub>As cell. FCA reduces the SE at relatively low emitter temperatures (i.e., by 12% at 800 K), whereas the loss is less than 1% at > 1250 K.

Figure S6 (see the Supporting Information) shows the current density (J) - voltage (V) characteristics measured under illumination by a SiC emitter <sup>16</sup>, with  $T_h$  varied from 914 K to 1425 K. From these data, we extract the series resistance of  $R_s = 6.7 \text{ m}\Omega \cdot \text{cm}^2$ , shunt resistance of  $R_{sh} = 14 \text{ k}\Omega \cdot \text{cm}^2$ , and diode ideality factor of 1.12. The electrical parameters and emitter temperatures are summarized in Table 1. The open circuit voltage  $V_{oc}$  exhibits a 140 mV loss relative to the radiative limit, which is calculated using <sup>22</sup>:

$$\frac{V_{oc}}{E_g} = 1 - \frac{T_c}{T_h} + \frac{k_B T_c}{E_g} \ln\left(\frac{T_h}{T_c}\right). \tag{1}$$

From the electrical and optical measurements, we calculate the PCE vs.  $T_h$  in Fig. 3(c). The circle and star data points denote the PCE of the single-cavity mode  $In_{0.53}Ga_{0.47}As$  ABTPV cell calculated using the simulated and measured SE, respectively. The maximum PCE is 31.7  $\pm$  0.1% ( $T_h$  = 1279 K) and 33.2  $\pm$  0.1% ( $T_h$  = 1352 K) using the simulated and measured SE, respectively. While FCA introduces a loss in PCE, it is insignificant for an optimized PCE at  $T_h$  > 1200 K. The buckled TPV cell has a lower SE than that of a flat cell, resulting in a lower PCE. The red line shows a significant PCE loss ranging from 6.5–10.2%, depending on the emitter temperature, in comparison to a flat TPV cell. Extrinsic loss sources such as shunt paths and series resistance account for majority of the PCE penalty between experiment and the radiative limit  $^{23,24}$ . We also provide the PCE that assumes the  $In_{0.53}Ga_{0.47}As$  current-voltage characteristics similar to those of Tervo *et al*  $^{19}$ , and based on a device model in the Supporting Information. The projection shows that a PCE = 40.0% and 40.2% at  $T_h$  = 1523 K is possible when FCA is included or neglected, respectively.

# **Conclusion**

We demonstrate a flat  $In_{0.53}Ga_{0.47}As$  ABTPV cell that supports only a single cavity mode in the air gap between the semiconductor membrane and the Au BSR. Compared to a buckled cavity, there is a 14.7 % to 33.6 % improvement (absolute) in the spectral efficiency over the range of emitter temperatures considered. When weighted to a 1352 K blackbody spectrum,  $R_{OOB} = 98.9 \pm 0.1\%$  for the flat cell, revealing that a single cavity mode is important to achieve a near perfect  $R_{OOB}$ . The buckled TPV cell shows a SE from 33.5 % to 58.9 % at  $T_h$  from 900 K to 1500 K. The flat TPV cell demonstrates SE from 68.6 % to 76.5 % at the same  $T_h$ , which exceeds that of previous  $In_{0.53}Ga_{0.47}As$  TPV cells, leading to a PCE = 31.7  $\pm$  0.1 % at  $T_h$  = 1352 K. This work provides guidance for the design of TPVs with a range of semiconductor

bandgaps, demonstrating that a flat, thin-film TPV membrane can realize a higher PCE than 40% by achieving a single-cavity mode within an air-bridge architecture.

#### Methods

**ABTPV cell fabrication.** The TPV film was grown on an InP wafer by solid source MBE (Veeco GENxplor). The In<sub>0.53</sub>Ga<sub>0.47</sub>As and InP epilayers were transferred to a Si substrate by a Au-Au cold-welding process <sup>18, 25</sup>, where the patterned Au layer on the TPV film forms an air bridge. The InP wafer was selectively removed by HCl wet-etching. The circular-mesa structure was defined by dry-etching by inductively coupled plasma (ICP)-reactive ion etching (gas flow rates of CH<sub>4</sub>:H<sub>2</sub> = 45:5 SCCM, RF power 150W). The mesa diameters are 170, 240, and 280  $\mu$ m. Following ICP etching, the sample was treated by wet chemical cleaning in HCl:H<sub>2</sub>O=1:1 and H<sub>2</sub>PO<sub>4</sub>:H<sub>2</sub>O<sub>2</sub>:H<sub>2</sub>O=1:1:8 for 10 s, respectively, to ensure smooth sidewalls. A Pt/Ti/Pt/Au (9/15/9/300 nm) liftoff metallization was applied to define the top metal contact ring. The sample was passivated by a polyimide coating (DuPont PI-2555) and consecutively cured at 100 °C for 10 min and 200 °C for 1 h. The polyimide on the mesa was etched by an O<sub>2</sub> plasma. Finally, the Ti/Au (10/200 nm) contact was patterned using liftoff.

**Diode Imaging.** The TPV cells were examined using an optical microscope (Olympus BX 51, Olympus, Japan), a 3D confocal laser microscope (LEXT OLS4000, Olympus, Japan), and a surface profiler (Dektak, Bruker, Germany). FTIR measurements were performed using an Agilent Cary 670-IR spectrometer (coupled to a Cary 620 FTIR microscope) with a 15× objective and a 128 × 128 MCT focal plane array detector (Agilent Technologies, CA). All data were collected at a 1 cm<sup>-1</sup> spectral resolution.

**Diode Characterization.** The TPV cell was mounted on a customized water-cooling stage, maintaining the temperature at 20 °C <sup>16</sup>. A SiC globar emitter (SLS203, Thorlabs Inc.) was

installed on a three-axis translational stage and centered on the cell. The current density-voltage characteristics were measured using a Keithley 2401 Source Measure Unit in the 4-wire sensing mode.

### ASSOCIATED CONTENT

**Supporting Information.** Simulation of light absorption and current-voltage curves, the hall effects in InP thin films, flat InGaAs membranes with different sizes, simulation of reflectance for multiple cavity modes, Fourier transform infrared measurements and simulations, current-voltage characterization of the unbuckled InGaAs TPV cell, TCAD modeling for an improved InGaAs TPV cell, and the calculation of spectral efficiency.

## **AUTHOR INFORMATION**

# **Corresponding Author**

Stephen R. Forrest – Department of Electrical Engineering and Computer Science, University of Michigan, Ann Arbor, Michigan 48109, United States; Department of Physics, University of Michigan, Ann Arbor, Michigan 48109, United States; orcid.org/0000-0003-0131-1903; Email: stevefor@umich.edu

### **Authors**

**Jihun Lim** – Department of Electrical Engineering and Computer Science, University of Michigan, Ann Arbor, Michigan 48109, United States; orcid.org/0000-0003-4074-9617

**Bosun Roy-Layinde** – Department of Chemical Engineering, University of Michigan, Ann Arbor, Michigan 48109, United States;

Bin Liu – Department of Electrical Engineering and Computer Science, University of

Michigan, Ann Arbor, Michigan 48109, United States;

**Lenert Andrej** – Department of Chemical Engineering, University of Michigan, Ann Arbor,

Michigan 48109, United States; orcid.org/0000-0002-1142-6627

**ACKNOWLEDGEMENTS** 

The authors acknowledge the Lurie Nanofabrication Facility at the University of Michigan for

semiconductor fabrications. This research was sponsored by the Army Research Office (ARO)

under Grant Number W911NF-18-1-0004 and the National Science Foundation (NSF) under

Grant Number 2018572. The views and conclusions contained in this document are those of

the authors and should not be interpreted as representing the official policies, either expressed

or implied, of the ARO or the U.S. Government. The U.S. Government is authorized to

reproduce and distribute reprints for Government purposes notwithstanding any copyright

notation herein.

**Conflict of Interest** 

The authors do not have any conflict of interest to disclose.

Date availability statement

The data that support the findings of this study are available from the corresponding author

upon reasonable request.

9

Table 1. Electrical parameters used in Fig. 3(c). Standard deviations are calculated from five separate measurements at each emitter temperature. The view factor (the ratio of overlap of the emitter and detector areas) is 0.27.

| $T_h(K)$ | V <sub>oc</sub> (mV) | $J_{sc}$ (mA/cm <sup>2</sup> ) | FF (%)    | $P_{out}$ (W/cm <sup>2</sup> ) | PCE (circles) (%) |
|----------|----------------------|--------------------------------|-----------|--------------------------------|-------------------|
| 914      | 309.5                | 4.3                            | 66.5      | 0.9                            | 18.7              |
|          | $\pm 0.8$            | ± 0.0                          | $\pm 0.4$ | ± 0.0                          | ± 0.2             |
| 987      | 351.7                | 16.0                           | 67.0      | 3.9                            | 23.5              |
|          | $\pm 0.6$            | ± 0.1                          | $\pm 0.4$ | $\pm 0.0$                      | ± 0.3             |
| 1060     | 380.9                | 42.6                           | 72.1      | 11.7                           | 26.9              |
|          | $\pm 0.4$            | ± 0.1                          | $\pm 0.2$ | $\pm 0.0$                      | $\pm 0.1$         |
| 1133     | 403.5                | 91.1                           | 73.2      | 26.9                           | 29.3              |
|          | $\pm 0.4$            | ± 0.1                          | $\pm 0.2$ | $\pm 0.1$                      | ± 0.2             |
| 1206     | 421.8                | 168.9                          | 73.7      | 52.5                           | 30.8              |
|          | $\pm 0.4$            | ± 0.1                          | ± 0.2     | ± 0.2                          | ± 0.1             |
| 1279     | 434.5                | 281.5                          | 73.7      | 90.2                           | 31.7              |
|          | $\pm 0.3$            | ± 0.1                          | $\pm 0.1$ | $\pm 0.2$                      | ± 0.1             |
| 1352     | 445.4                | 434.4                          | 72.4      | 140.2                          | 31.7              |
|          | $\pm 0.2$            | ± 0.3                          | $\pm 0.1$ | $\pm 0.4$                      | $\pm 0.1$         |
| 1425     | 454.0                | 633.4                          | 70.5      | 202.6                          | 18.7              |
|          | $\pm 0.2$            | ± 0.8                          | $\pm 0.1$ | ± 0.5                          | ± 0.2             |

### References

- (1) Ahmadi, M. H.; Ghazvini, M.; Sadeghzadeh, M.; Alhuyi Nazari, M.; Kumar, R.; Naeimi, A.; Ming, T. Solar power technology for electricity generation: A critical review. *Energy Science & Engineering* **2018**, *6* (5), 340-361.
- (2) Zabed, H.; Sahu, J.; Suely, A.; Boyce, A.; Faruq, G. Bioethanol production from renewable sources: Current perspectives and technological progress. *Renewable and Sustainable Energy Reviews* **2017**, *71*, 475-501.
- (3) Luque, R.; Herrero-Davila, L.; Campelo, J. M.; Clark, J. H.; Hidalgo, J. M.; Luna, D.; Marinas, J. M.; Romero, A. A. Biofuels: a technological perspective. *Energy & Environmental Science* **2008**, *1* (5), 542-564.
- (4) Mekhilef, S.; Saidur, R.; Safari, A. A review on solar energy use in industries. *Renewable and sustainable energy reviews* **2011**, *15* (4), 1777-1790.
- (5) Panwar, N.; Kaushik, S.; Kothari, S. Role of renewable energy sources in environmental protection: A review. *Renewable and sustainable energy reviews* **2011**, *15* (3), 1513-1524.
- (6) Kannan, N.; Vakeesan, D. Solar energy for future world:-A review. *Renewable and sustainable energy reviews* **2016**, *62*, 1092-1105.
- (7) Green, M. A.; Cells, S. Operating Principles, Technology and System Applications. *Sol. Cells* **1982**, 81-82.
- (8) Fraas, L.; Avery, J.; Huang, H.; Martinelli, R. Thermophotovoltaic system configurations and spectral control. *Semiconductor Science and Technology* **2003**, *18* (5), S165.
- (9) Coutts, T. A review of progress in thermophotovoltaic generation of electricity. *Renewable* and sustainable energy reviews **1999**, 3.
- (10) Swanson, R. M. Recent developments in thermophotovoltaic conversion. In 1980 International Electron Devices Meeting, 1980; IEEE: pp 186-189.

- (11) Song, J.; Choi, M.; Lim, M.; Lee, J.; Lee, B. J. Comprehensive analysis of an optimized near-field tandem thermophotovoltaic converter. *Solar Energy Materials and Solar Cells* **2022**, *236*, 111522.
- (12) Omair, Z.; Scranton, G.; Pazos-Outón, L. M.; Xiao, T. P.; Steiner, M. A.; Ganapati, V.; Peterson, P. F.; Holzrichter, J.; Atwater, H.; Yablonovitch, E. Ultraefficient thermophotovoltaic power conversion by band-edge spectral filtering. *Proceedings of the National Academy of Sciences* **2019**, *116* (31), 15356-15361.
- (13) Sun, X.; Silverman, T. J.; Zhou, Z.; Khan, M. R.; Bermel, P.; Alam, M. A. Optics-based approach to thermal management of photovoltaics: selective-spectral and radiative cooling. *IEEE Journal of Photovoltaics* **2017**, *7* (2), 566-574.
- (14) Park, K.; King, W. P. Performance analysis of near-field thermophotovoltaic devices considering absorption distribution. In *RADIATIVE TRANSFER-V. Proceedings of the Fifth International Symposium on Radiative Transfer*, 2007; Begel House Inc.
- (15) Burger, T.; Fan, D.; Lee, K.; Forrest, S. R.; Lenert, A. Thin-film architectures with high spectral selectivity for thermophotovoltaic cells. *ACS Photonics* **2018**, *5* (7), 2748-2754.
- (16) Fan, D.; Burger, T.; McSherry, S.; Lee, B.; Lenert, A.; Forrest, S. R. Near-perfect photon utilization in an air-bridge thermophotovoltaic cell. *Nature* **2020**, *586* (7828), 237-241.
- (17) Lee, B.; Lentz, R.; Burger, T.; Roy-Layinde, B.; Lim, J.; Zhu, R. M.; Fan, D.; Lenert, A.; Forrest, S. R. Air-bridge Si thermophotovoltaic cell with high photon utilization. *ACS Energy Letters* **2022**, *7* (7), 2388-2392.
- (18) Lim, J.; Fan, D.; Lee, B.; Forrest, S. R. Understanding and Control of Compressively Buckled Semiconductor Thin Films. *Physical Review Applied* **2021**, *16* (6), 064010.
- (19) Tervo, E. J.; France, R. M.; Friedman, D. J.; Arulanandam, M. K.; King, R. R.; Narayan, T. C.; Luciano, C.; Nizamian, D. P.; Johnson, B. A.; Young, A. R. Efficient and scalable GaInAs thermophotovoltaic devices. *Joule* **2022**, *6* (11), 2566-2584.

- (20) Baillargeon, J.; Cho, A.; Fischer, R.; Pearah, P.; Cheng, K. Growth of silicon and beryllium doped InP by MBE using solid phosphorus. In *Proceedings of 1994 IEEE 6th International Conference on Indium Phosphide and Related Materials (IPRM)*, 1994; IEEE: pp 148-150.
- (21) Postigo, P. A.; Dotor, M. L.; Huertas, P.; Golmayo, D.; Briones, F. Electrical and optical properties of undoped InP grown at low temperature by atomic layer molecular beam epitaxy. *Journal of Applied Physics* **1995**, *77* (1), 402-404.
- (22) Baldasaro, P.; Raynolds, J.; Charache, G.; DePoy, D.; Ballinger, C.; Donovan, T.; Borrego, J. Thermodynamic analysis of thermophotovoltaic efficiency and power density tradeoffs. *Journal of Applied Physics* **2001**, *89* (6), 3319-3327.
- (23) Lim, J.; Lee, B.; Roy-Layinde, B.; Lenert, A.; Forrest, S. Energy conversion efficiency limits of air-bridge thermophotovoltaic cells. *Bulletin of the American Physical Society* **2023**.
- (24) Lim, J.; Forrest, S. R. Limits to the Energy-Conversion Efficiency of Air-Bridge Thermophotovoltaics. *Physical Review Applied* **2023**, *19* (3), 034099.
- (25) Fan, D.; Lee, K.; Forrest, S. R. Flexible thin-film InGaAs photodiode focal plane array. *ACS Photonics* **2016**, *3* (4), 670-676.

## Figure captions

Figure 1. (a) Schematic of an  $In_{0.53}Ga_{0.47}As$  thin-film air-bridge (AB) thermophotovoltaic (TPV) cell. The thin-film membrane is buckled with multiple cavity modes.  $t_{air}$  is the air-bridge thickness and  $t_{buck}$  is the buckling height. (b) Top: 3D confocal laser microscope image of the buckled ABTPV surface. *Bottom*: Measured surface profile. (c) Top: Measured reflectance using Fourier transform infrared spectroscopy (FTIR). *Middle* and *bottom*: Simulated reflectances assuming a buckled and a flat TPV membrane, respectively.

Figure 2. (a) Schematic of a flat In<sub>0.53</sub>Ga<sub>0.47</sub>As ABTPV cell. (b) Optical microscope image of the flat cell. The dashed line delineates the air-bridge region. (c) Surface profile scanned through the center of the cell, as indicated by the white dashed line in the inset image obtained using confocal laser microscopy.

Figure 3. (a) Measured (blue circles) and simulated (red solid line) reflectance of the flat ABTPV cell. The shaded region indicates the simulated reflectance for the flat ABTPV cell. The black dashed line is from the experimental data in Fig. 1(c). (b) Spectral efficiency (SE) vs. emitter temperature. The dashed lines are the simulated SE for the flat ABTPV cell, where the shaded region is the SE loss by FCA. The solid lines are the minimum to maximum ranges of the measured SE for the flat ABTPV cell (see the Supporting Information). The dashed-dot line indicates the experimental SE for the buckled ABTPV cell. The symbols are from Refs. <sup>12, 16</sup>. (c) Power conversion efficiency (PCE) of the ABTPV cell vs. emitter temperature. Stars indicate the PCE inferred from the simulated SE for the flat ABTPV cell in (b), respectively. The dashed line is a guide to the eye. The red solid line is the PCE for the buckled ABTPV in (b). The improvement in PCE assumes that the diode has a higher *Voc* due to reduced radiative

recombination (see the Supporting Information). The blue color-filled region is the PCE loss due to FCA.

Figure 1

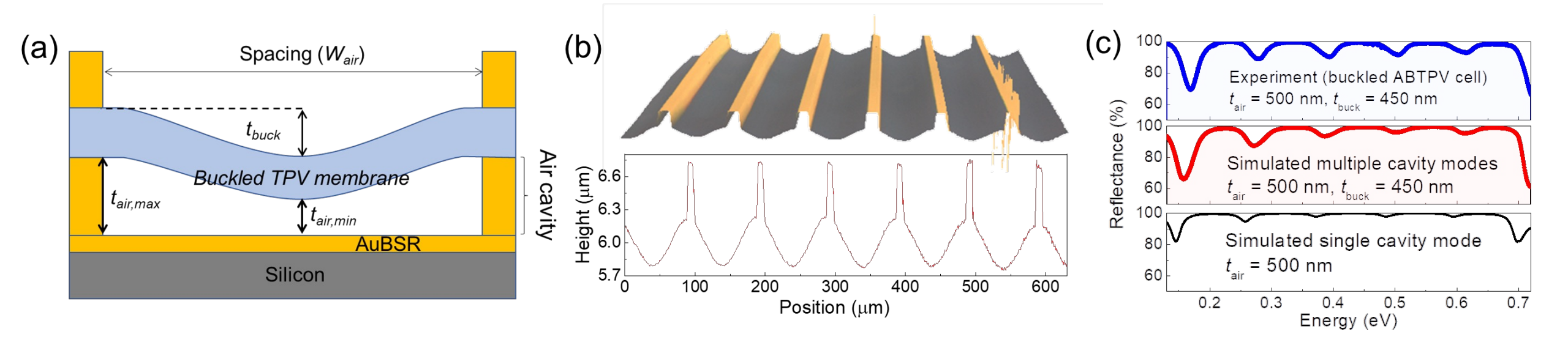


Figure 2

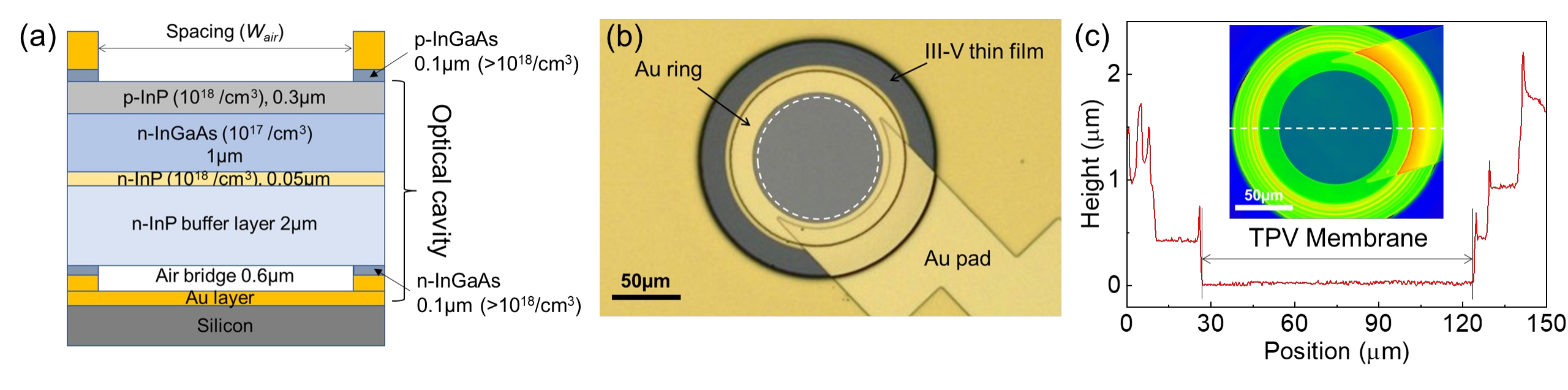


Figure 3

